

UNCLASSIFIED

Defense Technical Information Center
Compilation Part Notice

ADP011805

TITLE: Nanostructured Coatings of Inner Surfaces in Microporous Matrixes

DISTRIBUTION: Approved for public release, distribution unlimited

This paper is part of the following report:

TITLE: NATO Advanced Research Workshop on Nanostructured Films and Coatings. Series 3. High Technology - Volume 78

To order the complete compilation report, use: ADA399041

The component part is provided here to allow users access to individually authored sections of proceedings, annals, symposia, etc. However, the component should be considered within the context of the overall compilation report and not as a stand-alone technical report.

The following component part numbers comprise the compilation report:

ADP011800 thru ADP011832

UNCLASSIFIED

NANOSTRUCTURED COATINGS OF INNER SURFACES IN MICROPOROUS MATRIXES.

Yu.A. KUMZEROV

*A.F.Ioffe Physico-Technical Institute, Russian Academy of Sciences,
194021 St.Petersburg, Russia*

1. Introduction

There is growing interest in the physical properties of extremely small structures. The experimental realisation of new effects relies on the ability to create new types of structures and devices. Our understanding of material processing in the pursuit of ultra-small structures is continually advancing. Sophisticated epitaxial growth and lateral microstructuring techniques have made it possible to realise low-dimensional electronic systems with quantum confined energy structure i.e. quantum wells, quantum wires and quantum dots. Low-dimensional systems can also be obtained by confining a solid or liquid within the nanometer-sized pores of different porous materials (see [1]). Systems with size-selected nanoparticles embedded in a porous matrix via chemical coating have received some attention these past few years. In this case the confined materials penetrate into the pores due to wetting processes. In the case of non-wetting there is the possibility of using a mechanical coating of inner surfaces of porous materials when some external pressure forces non-wetting liquid into the pores [2]. Mechanical coating means that the mechanical energy of the piston forcing the liquids into the pores transforms to the energy of some new surface arising due to filling process (Fig.1). Since the total surface energy is proportional to the highly developed inner surface of the porous matrix, to surface tension of embedded materials and inversely proportional to the characteristic diameters of pores, for very small diameters a relative amount of surface energy may be very large and even comparable with some traditional sources of energy (Fig.1). For example, liquid mercury embedded into the pores of zeolites (needed pressure is about 20 kbars) accumulates of about 0.4 kJ/g mechanical energy in the form of a surface energy. Such a situation may be used for mechanical energy accumulation [3]. On the other hand the materials coating the inner surfaces of the pores in different porous matrixes may be interesting themselves as some physical objects with the characteristic sizes in nanometre scale i.e. as some new types of nanostructures. The advantages of such nanostructures are connected with the possibility to produce the following:

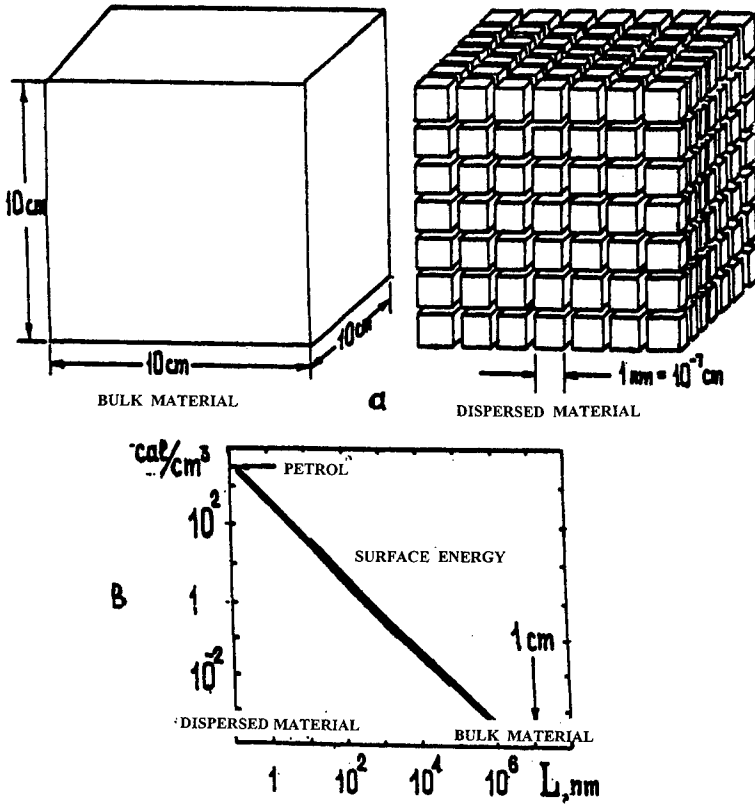


Figure 1. a) Surface arising due to process of material dispersion.

b) Surface energy per cm^3 of dispersed material versus characteristic size of dispersed particles

- nanostructures with different geometries (two-dimensional film-like structures, one-dimensional wire-like structures, zero-dimensional small particles-like structures).

- nanostructures with a large range of characteristic sizes (from approximately 1 nm to approximately 100-150 nm).

- nanostructures with very large total amount of nanomaterial (up to some cubic cm). Such situations permit the use some experimental methods (neutron scattering, heat capacity measurements) that require a large amount of nanostructures.

- nanostructures from different substances (from metals, including superconductors, from semiconductors, from insulators, including ferroelectrics etc). Further, examples of such nanostructures, and their physical properties will be presented.

2. Irregular systems of small particles in porous glasses.

Small particles or film-like objects can be obtained by confining a solid or liquid within the nanometer-sized pores of porous glasses. Porous silica glasses have often been used for this purpose because of their relatively well-characterised pore structure, large specific pore volumes and availability over several orders of magnitude in the mean pore diameter (about their structure see [4]). The porous matrix usually is prepared from a sodium borosilicate glass. This glass is produced from a melt of 75% SiO_2 , 20% B_2O_3 and 5% Na_2O . Heat treatment leads to a separation in a silicon-rich phase and a boron-rich one. After removing the boron-rich phase, there remains an interconnected solid skeleton of nearly pure SiO_2 with a rather homogeneous distribution of mass and pores. The pores have a rather narrow size distribution and the pore diameters may be varied from 4 nm to about 100 nm. The pores together with narrow necks, which connect the pores, form a random interconnected network in a glass bulk.

Phase transitions in materials confined within porous glasses have been studied intensively. The melting and freezing within porous glasses have been observed for materials such as water, organic liquids [5,6], metals with low melting point [7-11], helium [12], oxygen and some other simple liquids [13-15]. The ferroelectric phase transition within porous glass has been observed for NaNO_2 and K_2HPO_4 [16,17]. Superconductivity for some metals confined within porous glass has also been observed [18].

3. Regular systems of small particles in opals.

The regular systems of identical nanoparticles may be obtained by confining some substances within the pores of opal. Opal itself consists of identical silica balls with diameters (D) ranging from 150 to 350 nm (about its structure, see [19]). The size homogeneity of these spheres allows their assembly in a close three-dimensional lattice, usually with FCC symmetry. Empty voids exist between neighbouring balls which, in turn, form their own regular lattice. There are two types of interpenetrating voids in the opal lattice: eight-fold co-ordinated large voids each connected with eight four-fold co-ordinated small voids. A large void has the form of a truncated tetrahedron with four windows to four large voids. The diameters of spheres inscribed in the larger and smaller voids are $d_1=0.41D$ and $d_2=0.23D$ respectively. The diameter of a circle inscribed in the triangular window is $d_3=0.15D$. The density of voids in opal is typically 10^{14}cm^{-3} . The porosity of the ideal package of balls is 26% of the whole volume.

This matrix itself is interesting as a material for so-called photonic crystals, that behave with respect to photons like a dielectric crystal does with respect to electron

waves and demonstrates the photonic gap phenomenon [20]. The lattices of nanosize metal particles may be prepared by impregnation of the opal matrix by molten metal under high hydrostatic pressure conditions [21-25]. The shape of the metal grains is a precise copy of the void configuration since the metal occupies all free matrix volume. Thus, a three-dimensional metal replica of the matrix is formed. According to the matrix structure, each section consisting of two adjacent grains contains a constricted region which may be considered as a weak link i.e. the element of S-c-S (S-superconductor, c- constriction) type. Owing to the matrix these elements are arranged in a crystalline manner and form a macrosystem. The density of weak links in this material is near 10^{14}cm^{-3} . Defects of this secondary lattice are the same as those of ordinary atomic crystals, and therefore the samples are polycrystals consisting of crystallites with characteristic size near 0.01 cm [23]. This object demonstrated properties characteristic of the Josephson systems [21, 23, 24]. The oscillating dependence of the critical current magnitude on the external magnetic field for such samples was observed and its example is shown in Fig.2 (from [23]). Such dependence may be connected with a regular structure of investigated materials.

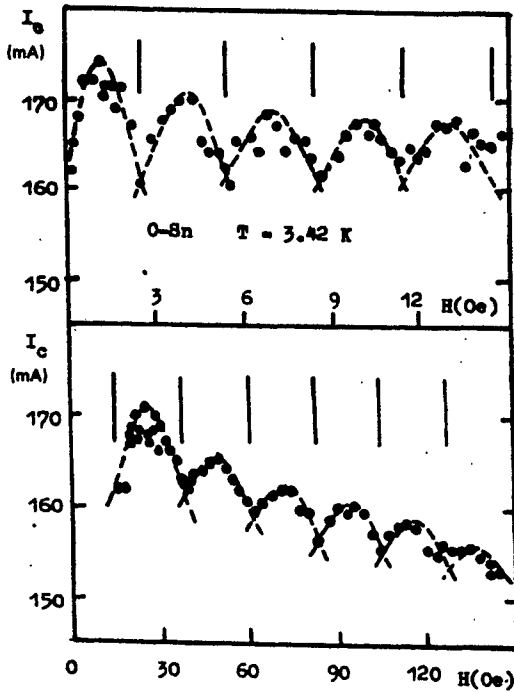


Figure 2. Critical current (I_c) vs magnetic field (H) for Sn-based sample. The upper plot corresponds to narrow and the lower plot to the wide scale of the magnetic field. The measured points are connected by lines to guide the eye. The sections indicate the periodicity.

4. Nanoclusters in zeolites.

The further type of microporous materials are the crystalline framework solids such as zeolites (about their structure, see [26]), that have found great utility as catalysts and sorption media because of their large internal surface area. They have regular arrays of identical voids, forming three-dimensional channel networks with very small sizes compared with the diameters of the atoms. For example, the channels in NaA zeolite have maximum diameter of 11.4Å, run in three perpendicular directions, and are interrupted by narrow diaphragms having a diameter 4.2Å. The cavities in NaX zeolite form a diamond lattice and have a maximum diameter of 13Å, the diaphragms have a diameter of 8Å.

Wetting liquids such as water will spontaneously fill the channels and cavities of zeolites essentially completely. It was shown in [27,28] that non-wetting liquids (mercury, gallium, bismuth) can be introduced into the regular channels of zeolites at sufficiently high pressures. The pressures at which mercury and gallium fill NaA zeolite are 14.5 kbar and 23 kbar, respectively. The critical pressures for NaX zeolite are 12.5 kbar (Hg) and 20 kbar (Ga). These values can be estimated from well-known porometric equation, based on the concepts of surface tension and wettability of liquid [27]

$$P_c = 0.4\sigma/d,$$

where P_c is critical pressure (kbar), σ is surface tension (dyn/cm) and d is the channel diameter (Å). After the external pressure is removed, some of the liquid metal leaves the zeolite channels. Nevertheless, the density of the zeolites shows that about half of the metal which was in the zeolite remains there. The rest of the metal collects in cavities and drops as a result of surface tension thus forming some ordered secondary crystal.

Some of the physical properties of such materials were investigated. For Hg and Ga drops a phase transition was observed [29]. It was manifested by singularities in the temperature dependence in the electrical conductivity and specific heat. The singularities were observed at temperatures much lower than the melting point of the bulk metal. It was concluded that the phase transition occurred in a system of interacting drops composed of metal atoms, and the interaction stabilised the system against fluctuations. The absorption spectra of Se drops in the zeolites NaA and NaX [30] were investigated. The form of the spectra obtained is typical of absorption spectra of crystals in the region of the optical absorption edge. It was concluded that the lattice of the clusters produced in the zeolite cavities is also a crystal, and the obtained spectral curves correspond to the absorption spectra of such cluster crystals in the region of the interband transitions.

A strong nonlinearity of the current-voltage characteristic of the cluster superlattice of tellurium in NaX zeolite was observed [31]. The characteristic was a series of current peaks rising in increasing amplitude in the field. This behaviour is

demonstrated in Fig.3 (from [31]). It was shown that these peaks appeared periodically when considered as a function of $1/E$ (E is electric field intensity). The periodicity of the current peaks (on the $1/E$ scale) of the current-voltage characteristic for Te in NaX zeolite was discussed on the basis of a theory of electrophonon resonance.

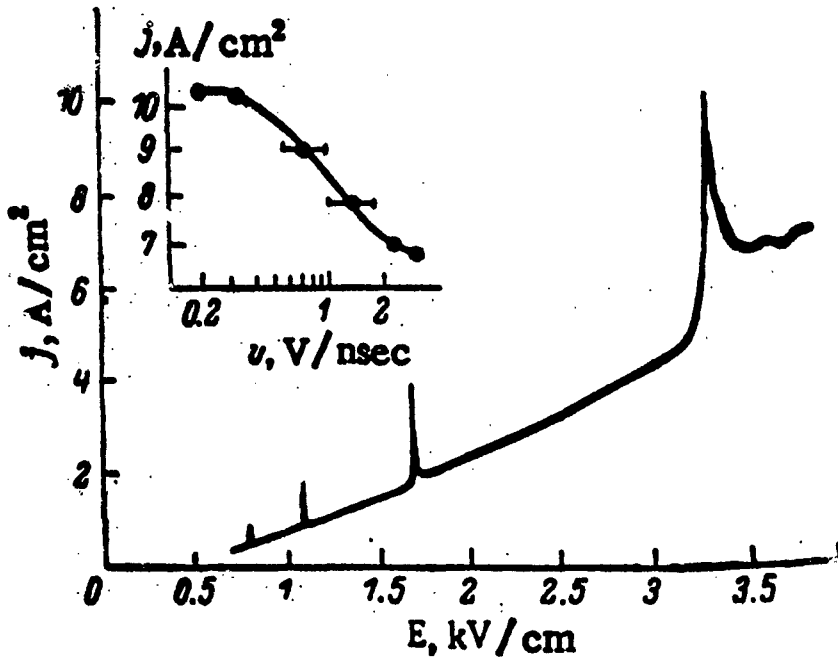


Figure 3. Oscillogram of the current-voltage characteristic obtained using sawtooth voltage pulses with a leading edge $\tau_r \sim 50$ nsec. The inset at the top of the figure gives the dependence of the amplitude of the $n=1$ peak on the rate of the rise of the voltage v .

5 Quantum wires in chrysotile asbestos.

Quantum wires of a wide class of materials can be prepared in porous matrices. This is natural chrysotile asbestos mineral (composition $Mg_3Si_2O_5(OH)_4$). It is a regular set of closely packed parallel ultrathin dielectric tubes with external diameters of ≈ 30 nm (this value determines the distance between the centres of the neighbour channels), and with internal channel diameters of 2-10 nm depending of the origin of the mineral ; its structure is described in [32, 33]. Chrysotile asbestos tubes constitute single-crystal alumino-silicate sheets (the thickness of one sheet is 7Å), which owing to their structural characteristics twist themselves into rolls until the radius of curvature of the outer and inner layers starts differing appreciably from their optimum value. The tubes of natural chrysotile asbestoses reach lengths of several centimetres.

When we fill the channels with molten materials (Hg, Sn, Bi, In, Pb, InSb, Se, Te) under high pressure conditions we have the possibility of obtaining a regular system of ultrathin parallel wires. Fig.4 demonstrates the model of this system. The reduction in the pressure of the molten metals after their introduction into the asbestos leads to a loss of sample conductivity on account of the oozing of the liquid metals from the channels; it is therefore essential to carry out the conductivity measurements directly under pressure, using the autonomous chamber with a reserve valve.

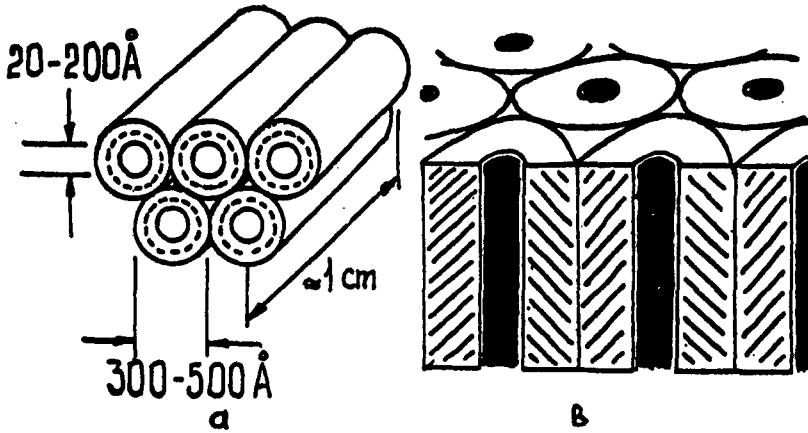


Figure 4. a) Close packed tubes of chrysotile asbestos.
b) System of ultrathin wires within the channels of chrysotile asbestos

The superconducting transitions of a complete series of such samples by the contact method were studied [34-40]. Particularly, the superconducting transition of metals in asbestos channels has a temperature spread that is due to fluctuations which are significant for such thin elements [35]. Fig.5 demonstrates such behaviour for mercury wires of 80 Å diameter. The measurements performed on mercury wires with diameters 20 Å [35] show that their superconducting transition is smeared from ~2K to ~6K that $\Delta T/T_c \sim 1$, where ΔT is the width of critical region. Some attempts of theoretical description of the fluctuation smeared superconducting transition are known [41-43] and the theoretical dependence is shown in Fig.5 by the solid line. It may be seen that the theoretical curve in the low temperature region is quite consistent with the experimental data. The critical temperature of the ultrathin wires was determined from resistance dependence on temperature, using some theoretical description of the fluctuation smeared superconducting transition [40]. Critical temperatures vs diameter were measured for mercury, tin and indium with wires from 20 Å to 150 Å. They are demonstrated in Fig.6. The critical temperature of tin wires increases with decreasing diameter and critical temperature on diameter dependence.

for mercury and indium wires have a maximums at 4.6K for diameter $\approx 40\text{\AA}$ (Hg) and at 6.2K for diameter $\approx 20\text{\AA}$ (In).

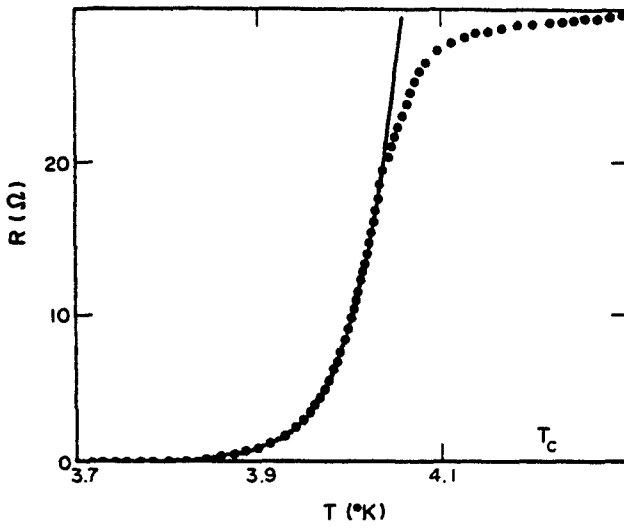


Figure 5. Resistance as a function of temperature for mercury wires of 80Å diameter in the superconducting region

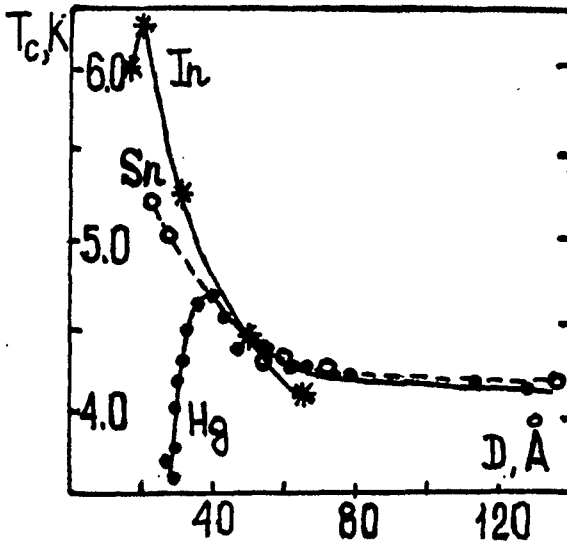


Figure 6. Superconducting critical temperature dependence on the diameter of mercury, tin and indium wires.

Some increase of resistance and non-linearity of current-voltage characteristics with decreasing temperature were observed on mercury ultrathin wires [35,44]. The temperature dependence of mercury 25A wires resistance in the region below 60K is shown in Fig.7. In the temperature range 10-60K the experimental data are well described by $T^{-3/2}$ dependence. Below 10K the

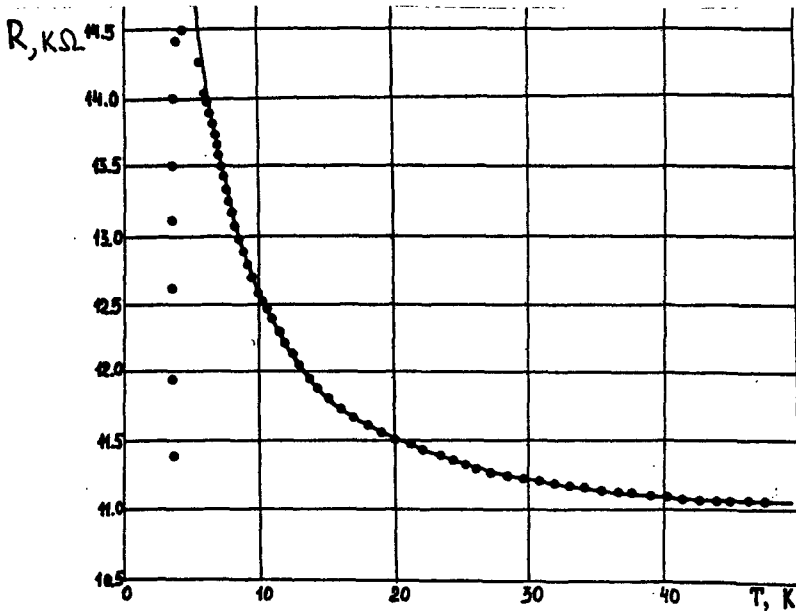


Figure 7. The dependence of resistance of 25A mercury wires on temperature (the solid line corresponds to $\Delta R/R \sim T^{-3/2}$ dependence).

superconducting fluctuations dominate the conductivity. As to wires with larger diameters, their negative temperature derivative of resistivity decreases with the diameter. These results were explained as the display of localisation effects in disordered one-dimensional system. The temperature dependence of resistivity of thin wire due to localisation (one-dimensional case) can be written as [46]

$$R = R_0 [1 + \rho_B (D\tau_i)^{1/2} / R_T d^2]$$

where ρ_B is the impurity scattering resistivity, $D = v_F l / 3$ is the diffusion constant, v_F is the Fermi velocity, $R_T = 36500 \Omega$, d is diameter of the wire, l is the elastic mean free path, τ_i is the inelastic scattering time. The necessary condition for one-dimensional behaviour is $d < (D\tau_i)^{1/2}$. The temperature dependence of wire resistance in this equation is governed by the temperature dependence of τ_i , so that $\Delta R/R_0 = (R - R_0)/R_0 \sim (\tau_i)^{1/2}$. Since we have $\Delta R \sim T^{-3/2}$ dependence, it follows that $\tau_i \sim T^{-3}$. Such temperature dependence of inelastic scattering time may be due to scattering on three-dimensional

phonons. Using this equation we find $\tau_i \sim 10^{-10}$ sec at 10K. The localisation length $(Dr_i)^{1/2}$ at 10K is about 3×10^{-5} cm which satisfies the localisation criterion for wires and so the data obtained may be interpreted in terms of one-dimensional electron localisation.

The melting and freezing as a first-order phase transition of mercury wires in the range between 20A and 100A [45] was investigated. The first-order phase transitions in dispersed systems have been studied considerably less extensively than the second-order phase transitions. There have been virtually no experiments of this type performed using approximately one-dimensional systems as objects of investigation. The melting region of extremely fine mercury wires was identified on the temperature curve of the resistance. It was of considerable interest to study this transition as a function of wire diameter. The samples whose wires had a small spread in diameter (not exceeding $\sim 5\%$) were chosen for measurements. The melting region extends over a large temperature interval, which is probably attributable to the fluctuations whose appreciable effect on the phase transitions in one-dimensional systems has been well established. At such a highly diffuse transition, it is not clear what point should be regarded as the melting point. Since there are no physically sound criteria for determining this point on the resistance versus temperature curve in the melting region (although these criteria can be determined for second-order phase transitions in several cases [40]), we can arbitrarily assume that the melting point is that point at which the resistance changes only half as much as it does during melting.

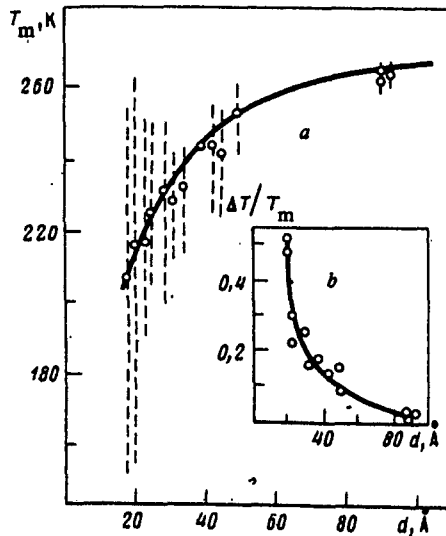


Figure 8. a) The melting point of extremely fine mercury wires versus the diameter (dashed line corresponds to the diffuse-transition region).
b) The diffusive melting range versus diameter

The dependence of a particular melting point on the diameter is shown in Fig.8. Also shown here is the region in which the transition becomes diffuse (dashed lines). The solid curve corresponds to the dependence $T=T_0(1-d^*/d)$, where $d^*\sim 5.5\text{\AA}$ and $T_0\sim 280\text{K}$, which is equal to the melting point of bulk mercury at a pressure of ~ 10 kbar. Fig.2b is a plot of $\Delta T/T_m$ (ΔT is the diffuse-transition region) as a function of the diameter, and the solid curve corresponds to the relation $\Delta T/T_m=(D/d)^2$, where $D\sim 14\text{\AA}$.

In addition some optical properties of ultrathin wires incorporated within chrysotile asbestos nanotubes were studied. Polarised optical absorption spectra of Hg, Bi and InSb wires have been studied in the spectral region 0.5-3 eV, and high anisotropy of the absorption has been observed [47,48]. InP quantum wires have been produced in channels of asbestos by metal-organic chemical vapour deposition [49]. A comparative study of Raman, optical absorption, and photoluminescence spectra revealed the dependence of the optical properties of quantum wires on interface effects, namely, atomic interaction in the wires, wire-matrix, and wire-wire interactions.

6. Conclusions.

The results obtained clearly show good potential for the use of the natural and artificial microporous media for the preparation of the artificial systems that are interesting for scientific investigations and potential applications. The utilisation of porous glasses, artificial opals, and chrysotile asbestos matrices allows the formation of nanostructures for measurement of electrical, optical and other properties.

7. Acknowledgements.

This work has been partly supported by Programme «Physics of Nanostructures» (grant- 99-1112) and RFFI (grant 97-02-18267).

8. References.

1. Schwarz J.A. and Contescu C.I.(eds) (1999) *Surfaces of Nanoparticles and Porous Materials*, Marcel Dekker Inc.,New-York
2. Bogomolov V.N.(1978) Liquids within ultrathin channels, *Uspehi fizicheskikh nauk* **124**, 171-182
3. Bogomolov V.N.(1993) Surface energy and prospects for it use in power generation, transport and ecology, *Sov. Technical Physics*, **38**, 224-227

4. Levitz P., Ehret G., Sinha S.K., Drake J.M.(1991) Porous vycor glass: the microstructure as probed by electron microscopy, direct energy transfer, small-angle scattering, and molecular adsorption, *J.Chem.Phys.*, **95**, 6151-6161
5. Mu R. and Malhorta V.M.(1991) Effects of surface and physical confinement of the phase transitions of cyclohexane in porous silica, *Phys.Rev.***44B**, 4296-4303
6. Strange J.H., Raham M., Smith E.G.(1993) Characterisation of porous solids by NMR, *Phys.Rev.Lett.***71**,3589-3591
7. Borisov B.F., Charnaya E.V., Hoffmann W-D., Michel D., Shelyapin A.V. and Kumzerov Yu.A.(1997) NMR and acoustic investigations of the melting-freezing phase transition of gallium in a porous glass, *J.Phys.Condens.Matter* **9**, 3377-3386
8. Borisov B.F., Charnaya E.V., Kumzerov Yu.A., Radzhabov A.K., Shelyapin A.V.(1994) Phase transitions for gallium microparticles in a porous glass, *Sol.St.Comm.***92**, 531-533
9. Shabanova E., Charnaya E.V., Schaumburg K. and Kumzerov Yu.A.(1997) NMR studies of gallium embedded into a porous glass, *Physica* **B229**, 268-274
10. Kumzerov Yu.A., Nabereznov A.A., Vakhrushev S.B. and Savenko B.N.(1995) Freezing and melting of mercury in porous glass, *Phys.Rev.***B52**, 4772-4774
11. Charnaya E.V., Tien C., Lin K.J., Kumzerov Yu.A.(1998) X-ray studies of the melting and freezing phase transitions for gallium in a porous glass, *Phys.Rev.***58B**, 11089-11092
12. Beamish J.R., Mulders N., Hikata A. and Elbaum C.(1991) Vacancy diffusion and stress relaxation in ⁴He freezing in porous Vycor, *Phys.Rev.***B44**, 9314-9318
13. Molz E., Wong A.P.Y., Chan M.H.W. and Beamish J.R.(1993) Freezing and melting of fluids in porous glasses, *Phys.Rev.***B48**, 5741-5750
14. Warnock J., Awschalom D.D. and Shafer M.W.(1986) Geometrical supercooling of liquids in porous glass, *Phys.Rev.Lett.***57**, 1753-1756
15. Schindler M., Destinger A., Kondo Y. and Pobell F.(1996) Hydrogen in porous Vycor glass. *Phys.Rev.***B53**, 11451-11461
16. Colla E.V., Koroleva E.Yu., Kumzerov Yu.A., Savenko B.N., Vakhrushev S.B.(1996) Ferroelectric phase transitions in materials embedded in porous media, *Ferroelectric Letters* **20**, 143-147
17. Colla E.V., Fokin A.V., Kumzerov Yu.A.(1997) Ferroelectric properties of nanosize KDP particles, *Sol.St.Comm.* **103**, 127-130
18. Charnaya E.V., Tien C., Lin K.J., Kumzerov Yu.A.(1998) Superconductivity of gallium in various confined geometries, *Phys.Rev.* **B58**, 467-472
19. Balakirev V.G., Bogomolov V.N., Zhuravlev V.V., Kumzerov Yu.A., Petranovskii V.P., Romanov S.G., Samoilovich L.A. (1993) Three-dimensional superlattices within the matrixes of opal, *Kristallographia* **38**, 111-120
20. Bogomolov V.N., Gaponenko S.V., Germanenko I.N., Kapitonov A.M., Petrov E.P., Gaponenko N.V., Prokofiev A.V., Ponyavina A.N., Silvanovich N.I., samoilovich S.M. (1997) Photonic band gap phenomenon and optical properties of artificial opals, *Phys.Rev.* **55E**, 7619-7625
21. Bogomolov V., Zhuravlev V., Zhadorozhnii A., Kolla E., Kumzerov Yu. (1982) Voltage-current characteristics of regular system of weakly coupled superconducting particles, *JETP Lett.* **36**, 365-367
22. Bogomolov V.N., Kazantseva L.K., Kolla E.V., Kumzerov Yu.A.(1987) Periodic peaks of a resistive state during destruction of the superconductivity by a current in a lattice of weakly coupled indium particles, *Sov.Phys.Solid State* **29**, 359
23. Bogomolov V.N., Kumzerov Yu.A., Romanov S.G., Zhuravlev V.V. (1993) Josephson properties of the three-dimensional regular lattice of the weakly coupled nanoparticles, *Physica* **C208**, 371-384
24. Kumzerov Y., Bogomolov V., Colla E., Romanov S. (1994) Three-dimensional regular Josephson medium from identical nanoparticles, *Phys.Low-Dim.Struct.* **11/12**, 129-134

25. Babmuratov K.Kh., Zhuravlev V.V., Kumzerov Yu.A., Romanov S.G., Khachaturov S.A. (1993) Structure of a resistive superconducting transition in a regular lattice of indium nanoparticles, *Sov.Phys.Solid State* **35**, 795-797
26. Breck D.W. (1974) *Zeolite molecular sieves*, A Wiley-Interscience Publication John Wiley & Sons, New-York
27. Bogomolov V.N. (1972) Nonwetting liquids in ultrathin channels, *Sov.Phys.Solid State* **14**, 1048-1050
28. Bogomolov V.N., Zhadorozhnyi A.I. (1975) Monoatomic chains of Hg and Bi in mordenite and surface tension of liquid metals, *Sov.Phys.Solid State* **17**, 1078-1079
29. Bogomolov V.N., Volkonskaya T.I., Zadorozhnyi A.I., Kapanadze A.A., Lutsenko E.L. (1975) Phase transition in a system of Ga and Hg drops in zeolite cavities of 12A diameter, *Sov.Phys. Solid State* **17**, 1110-1112
30. Bogomolov V.N., Lutsenko E.L., Petranovskii V.P., Kholodkevich S.V. (1976) Absorption spectra of three-dimensionally-ordered system of 12A particles, *JETP Lett.* **23**, 482-484
31. Bogomolov V.N., Vaitekunas F.K., Zadorozhnyi A.I., Pavlova T.M., Sutkus K.V. and Yashin G.Yu. (1983) Determination of the time taken to establish a current flow regime in the region of N-type peaks of the current-voltage characteristic of an NaX-Se crystal, *Sov.Phys. Solid State* **25**, 1983-1984
32. Pundsak F.L. (1961) The pore structure of chrysotile asbestos, *J.Phys.Chem.* **65**, 30-33
33. Yada K. (1967) Study of chrysotile asbestos by a high resolution electron microscope, *Acta Cryst.* **23**, 704-707
34. Bogomolov V.N., Krivosheev V.K., Kumzerov Yu.A. (1972) Superconductivity of mercury in chrysotile asbestos, *Sov.Phys. Solid State* **13**, 3148-3150
35. Bogomolov V.N., Kumzerov Yu.A. (1975) Fluctuations in mercury filaments five atoms in diameter, *JETP Lett.* **21**, 198-200
36. Bogomolov V.N., Klushin N.A., Kumzerov Yu.A. (1977) Superconducting transition of indium filaments at 6K, *JETP Lett.* **26**, 72-74
37. Bogomolov V., Kumzerov Y., Pimenov V. (1981) Splitting of the heat capacity peak of metal filaments in a dielectric matrix in the superconducting region with decreasing diameter of the filaments, *Physics Letters* **86A**, 183-184
38. Bogomolov V.N., Kvyatkovskii B.E., Kolla E.V., Ktitorov S.A., Kumzerov Yu.A. and Okuneva N.M. (1981) N-type current-voltage characteristic of ultrathin metal filaments in the superconducting state, *Sov.Phys. Solid State* **23**, 1271-1272
39. Bogomolov V.N., Kolla E.V., Kumzerov Yu.A., Okuneva N.M., Prigodin V.N. (1980) Appearance of the dielectric instability and its coexistence with the superconductivity in ultrathin metallic filaments with decreasing diameter, *Sol.St.Comm.* **35**, 363-366
40. Bogomolov V.N., Kolla E.V., Kumzerov Yu.A. (1983) Determination of the critical temperature of the ultrathin metals filaments superconducting transition and its dependence on the filament diameter, *Sol.St.Comm.* **46**, 159-160
41. Langer J.S., Ambegaokar V. (1967) Intrinsic resistive transition in narrow superconducting channels, *Phys.Rev.* **164**, 498-510
42. McCumber D.E., Halperin B.I. (1970) Time scale of intrinsic resistive fluctuations in thin superconducting wires, *Phys.Rev.* **B1**, 1054-1070
43. Larkin A.I., Ovchinnikov Yu.N. (1973) Fluctuation conductivity in the vicinity of the superconducting transition, *J.Low Temp.Phys.* **10**, 407-421
44. Bogomolov V.N., Kolla E.V., Kumzerov Yu.A. (1983) One-dimensional effects in low-temperature conductivity of ultrathin metallic filaments, *Sol.St.Comm.* **46**, 383-384
45. Bogomolov V.N., Kolla E.V., Kumzerov Yu.A. (1985) First-order phase transition in an approximately one-dimensional system, *JETP Lett.* **41**, 34-37
46. Thouless D.J. (1980) The effect of inelastic electron scattering on the conductivity of very thin wires, *Sol.St.Comm.* **34**, 683-685

47. Kumzerov Y., Poborchii V. (1994) Ultrathin wires with near atomic diameters, *Phantoms Newsletter* 4, 2-3
48. Ivanova M.S., Kumzerov Y.A., Poborchii V.V., Ulashkevich Y.V., Zhuravlev V.V. (1995) Ultrathin wires incorporated within chrysotile asbestos nanotubes: optical and electrical properties, *Microporous Materials* 4, 319-322
49. Romanov S.G., Butko V.Yu., Kumzerov Yu.A., Yates N.M., Pemble M.I., Agger J.R., Anderson M.W., Sotomayor-Torres C.M. (1997) Interface phenomena and optical properties of structurally confined InP quantum wires ensembles, *Phys.Solid State* 39, 641-648